Bi-exponential ^{23}Na T$_2^*$ components analysis in the human brain

Frank Riemer[1,2], Bhavana S. Solanky[1], Claudia A. M. Wheeler-Kingshott[1] and Xavier Golay[2]

[1] Queen Square MS Centre, NMR Research Unit, Department of Neuroinflammation, UCL Institute of Neurology, London, UK.

[2] Department of Brain Repair and Rehabilitation, UCL Institute of Neurology, London, UK.

Correspondence to: Frank Riemer, Department of Radiology, Box 218, Cambridge Biomedical Campus, Cambridge CB2 0QQ, UK. Frank.Riemer.10@ucl.ac.uk

Abbreviations:

^{23}Na	-	Sodium-23
CSF	-	Cerebrospinal fluid
GM	-	Grey matter
K	-	Potassium
MQF	-	Multiple Quantum Filter
Na	-	Sodium
NaCl	-	Sodium chloride
NNLS	-	Non negative least squares
TSC	-	Total sodium concentration
WM	-	White matter

Abstract

Purpose:

To measure the sodium transverse relaxation time T_2^* in the healthy human brain.

Methods:

5 healthy subjects were scanned with 18 echo times as short as 0.17 ms. T_2^*s were fitted on a voxel-by-voxel basis using a bi-exponential model. Data was also analysed using a continuous distribution fit with a region-of-interest based inverse Laplace transform.

Results:

Average T_2^* values were 3.4 ± 0.2 ms and 23.5 ± 1.8 ms in white matter (WM), for the short and long components respectively, as well as 3.9 ± 0.5 ms and 26.3 ± 2.6 ms for the short and long components respectively in grey matter (GM) using the bi-exponential model. Continuous distribution fits yielded results of 3.1 ± 0.3 ms and 18.8 ± 3.2 ms in WM, for the short and long components respectively, as well as 2.9 ± 0.4 ms and 17.2 ± 2 ms for the short and long components respectively in GM.

Conclusion:

[23]Na T_2^* values of the brain for the short and long component for various anatomical locations using ultra-short echo times are presented for the first time.

Bi-exponential ^{23}Na T$_2^*$ components analysis in the human brain

Introduction

Total sodium (^{23}Na) measures in the brain provide an indirect indication of disease burden and previous work in the central nervous system found disease progression correlating with sodium concentration alterations in diseases such as Multiple Sclerosis, Alzheimer's and Huntington's.[1-3] However, when isolated, the intracellular ^{23}Na-fraction can be used to directly monitor cellular loss or Na-K pump malfunctioning, a more specific measure that would help understand the mechanisms in these diseases better.

Intracellular sodium is not directly accessible without toxic shift reagents or low resolution multiple quantum filtering techniques. As a spin 3/2 nucleus, ^{23}Na has 4 degenerate energy levels, leading to possible single, double and triple quantum transitions. While shift reagents are used to alter the chemical shift for the extracellular contribution to the signal, triple quantum filters aim to create triple quantum transitions arising from quadrupolar moment fluctuations and reject all signal from interstitial single and double quantum transitions. The triple quantum transitions are thought to arise from intracellular sodium environments exhibiting bi-exponential transverse relaxation only. It has been argued that triple quantum filtering can therefore be approached by suppression or subtraction of mono-exponential signal.[4,5] Recent studies have also demonstrated that more than half of the in vivo sodium triple quantum signal could be from extracellular space.[6] Since the triple quantum filtered signal is magnitudes smaller than that of single quantum transitions, nominal in vivo voxel sizes of 8-12 mm are common even at 7T.[7-9] Therefore, alternative ways to measure similar information would be worthwhile.

Proton (^{1}H) MRI T$_2$ and T$_2^*$ studies have been used in the past to interrogate different water environments, and an ultra-short component in the brain has been associated to myelin-water[10], previously not accessible to conventional ^{1}H-MRI imaging sequences. Similarly, accurate characterisation of the sodium T$_2$ could yield information on the environment of the sodium ions and if subtle changes are related to early disease processes.

In restricted single compartment environments, such as porous media, the ^{23}Na T$_2$ is dominated by single quantum transitions exhibiting bi-exponential relaxation properties with characteristic

amplitudes and ultra-short to short transverse relaxation times. Motional averaging, as seen in fluids, appears mono-exponential with long relaxation times and can therefore be clearly differentiated from the restrictive compartment. In the bi-exponential signal, the short T_2 component, which makes up 60 % of the signal has characteristically short transverse relaxation times of 0.5 to 5 ms, while the longer component, with a lower amplitude (40 %) has transverse relaxation times of 15 to 30 ms.[11,12] Dissolved sodium in the fluid phase, such as in saline has in comparison a transverse relaxation that appears mono-exponential, with T_2s of 30 - 60 ms.[11] The T_2 relaxation times can therefore reflect the environment of the sodium ions. Typical characterisation of T_2s is carried out using spin-echo experiments, which are inappropriate for the fast decays of interest here, as they tend to have effective TEs of 30 ms and longer. Alternatively, the transverse relaxation time T_2^*, which is composed of the T_2 time constant plus a small contribution from magnetic field inhomogeneities, can be measured using gradient echo sequences with UTE excitations and readouts. These magnetic field inhomogeneities that contribute to T_2^* are specific to the field strength and MR-system used, but are however negligible in the limit of short T_2s and the low gyromagnetic ratio of ^{23}Na.[13] Given these properties and the low SNR of Multiple Quantum Filter (MQF) techniques, here we aim to measure the effective transverse relaxation time T_2^* to interrogate the sodium relaxation properties of different tissue types within the human brain to provide an alternative way to investigate the underlying tissue environment.

In this study we present the first comprehensive analysis of WM and GM in a large range of anatomical locations covering both short and long echo times between 0.17 and 70.7 milliseconds to accurately characterise the transverse relaxation time properties of brain tissue, using both bi-exponential and multi-exponential continuous distribution fitting methods. Multi-exponential continuous distribution fitting is carried out using the inverse Laplace transform,[14,15] which to our knowledge has not been performed in ^{23}Na relaxometry before.

Experimental

Subjects

5 healthy subjects were recruited (mean age 29 years - 2 male, 3 female), who consented to the study approved by our local ethics committee. 2 cylindrical falcon tubes containing 33 and 66 mM NaCl in 4 % agar, as commonly used in quantification studies, were attached to the subjects' heads. These were also used for additional T_2^* estimates, as they have been shown to yield bi-exponential transverse relaxation akin to that of biological tissue.[16]

MRI protocol

All subjects were scanned on a Philips 3T Achieva system (Netherlands) using a fixed tuned sodium volume coil (Rapid Biomedical, Germany). [1]H imaging was performed on the MR-system's quadrature body coil.

[23]Na

All scans were performed using a 3D radial ultra-short echo time (UTE) "stack-of-stars" sequence, using an isotropic nominal voxel size of 5 mm, field of view of 240 mm and 40 slices with a repetition time (TR) of 120 ms, 250 Hz readout bandwidth per pixel and 134 readouts ("spokes") per slice. A multi-echo scan with 15 echo-times (TE) between 0.17 and 70.7 ms (ΔTE 4.7 ms) and three additional individual scans with echo times 0.3, 0.5 and 1 ms were performed to overcome the shortest ΔTE limitation imposed by the length of the FID readout and subsequent echo formation time. Figure 1 illustrates the sequence diagram for the multi-echo readout. After each excitation, slice-encoding is accomplished using phase encoding on G_z and a FID half-spoke is acquired after which full-spoke echoes are acquired with alternating polarities. In subsequent excitations G_x and G_y are incremented to sample different ranges of k_x and k_y. For echo times 0.3, 0.5 and 1 ms, 3 additional FID-only scans were acquired. A total of 18 echo times were used and the total sodium protocol time was 43 minutes.

[1]H

A proton-density (PD) weighted spin-echo [1]H (TE= 34 ms, TR= 3250 ms) scan with an in-plane resolution of 1 mm, 5 mm slice thickness and a 240 mm^2 FOV with 40 slices was performed on

the quadrature body coil on the subjects without repositioning. Including localiser, total duration of the ^{1}H protocol was 5 minutes.

Registration and Image processing

To account for movement during and between the individual scans, images were rigidly realigned using SPM8 (University College London, UK). Signal intensities were corrected slice-wise for low-SNR quadrature noise on the [23]Na images using Miller and Joseph's power image method, to avoid over-estimation of the fitted parameters, due to non zero-mean noise.[17]

Bi-exponential fixed fraction non-negative least squares fit

A non-negative least squares (NNLS) fit was implemented in Matlab 7.11 (the MathWorks, US), using a bi-exponential model with fixed amplitude fractions of 0.6 and 0.4 for the short and long components respectively,[11-12] resulting in a map of short and a map of long T_2^* components for each subject, as well as M_0 and residuals/noise only images.

ROIs for the fixed-fraction bi-exponential fit were placed in anatomically matched regions on the short and long T_2^*-component maps using Osirix 5.0.2 (Pixmeo Sarl, CH). ROI target areas were WM and GM in the major lobes, the cerebellum and cerebral cortex (GM only) using the [1]H-PD scan for tissue identification. Additional measures were taken in the known concentration agar phantoms from several slices. A total of 30 ROI measures in WM, 25 ROIs in GM and 5 ROIs each in of the phantoms were taken for each individual subject. ROI sizes ranged from 6 to 16 voxels.

Continuous distribution fit

The data was additionally analysed with a continuous distribution fit using a regularised inverse Laplace transform,[14] with no restriction on numbers of exponentials and associated amplitudes. The regularised inverse Laplace transform was computed using a least squares method in Matlab 7.0.11 (the MathWorks, US) based on Marino's implementation of Provencher's CONTIN program.[14,18] The estimation was carried out using the signal model:

$$y(TE) = \int_{t(\min)}^{t(\max)} g(s) \cdot e^{-TE/s} \, ds \qquad\qquad [1]$$

where *y(TE)* is the data measured at echo time TE, *g(s)* a vector of relaxation times s ranging from *t(min)* to *t(max)* with an initial guess weighting distribution $g_0(s)$. The solution of equation 1 is a spectrum of relaxation times *g(s)*. Relaxation times were regularised over 80 bins between the lower and upper bounds for the time constants *t(min)* and *t(max)*, corresponding to 0 and 100 ms respectively. Bins were logarithmically distributed between 0 and 15 ms over 50 bins. Longer components between 15 - 30 ms were binned with 1 ms separation, after which bins of 5 ms were used for T_2^* up to 100 ms, giving a total vector length of 80 bins. As part of the fitting routine, calculation was performed 16 times for each ROI varying a regulariser α ($0 < α < 1$, Δα=0.0825) in the optimization function that adjusts the number of independent components fitted. A modified F-test is then carried out to pick the regularization value (and therefore number of fitted components) that best describes the data. The best regularization value was regarded as the one that minimizes the *p* value of the modified F-test ($p < 0.05$); with the null hypothesis being that all fitted component amplitudes are zero.

In a second test, the regularization value was then regarded as stable if the next higher and next lower regularization value provided the same peak positions and amplitudes within 5 % difference. If this was not the case, the fit was rejected.[19-20]

The initial guess distribution *g(0)* had peaks centred around 2 and 20 ms, with relative amplitudes of 60 and 40 % to each other respectively, based on estimated T_2^*s for brain tissue.[11] An additional small amplitude component with 60 ms T_2^* was also included, to represent CSF contamination. See Figure 2 for a representation of the guess distribution.

Polygonal ROIs with an area of approximately 16 pixels each were placed in Matlab 7.0.11 (the MathWorks, US). Based on the ROIs used in the bi-exponential fit, a reduced number of ROIs were used in the continuous distribution fit, due to increased computational time for estimation of the distributions. A total of 16 ROIs in WM, 12 ROIs in GM and 5 ROIs in each phantom were used in the continuous distribution fit for each subject. Peak values only were picked for the relaxation time estimation and their associated amplitudes were used for the component amplitude estimation.

Statistics

Statistical analysis was performed in Matlab 7.0.11 (the MathWorks, US) using the statistics toolbox functions for balanced one-way analysis of variance (ANOVA) using Tukey's honestly significant difference criterion for multiple comparisons. A p-value of < 0.05 was considered statistically significant. P-value statistics were evaluated between WM, GM and phantom ROIs to assess any sodium T_2^*-differences based on tissue type and Na concentration.

Results

Figure 3 shows an exemplary mid-transverse section of the brain from one volunteer, over the range of echo times used, to illustrate the decay of the signal with increasing echo time.

Bi-exponential fit

Figure 4 shows assorted slices of the calculated short and long T_2^*-component maps from one volunteer. Noticeable is the reduced visibility of the cerebrospinal fluid in the short component maps; and likewise the skin of the skull and agar phantoms have largely disappeared from the long component maps.

Table 1 shows the summarised results averaged from the 5 volunteers for the two known concentration phantoms and all white and grey matter ROIs. While the standard deviation of the mean is small ($\leq$10%), results were not significantly different between the mean WM and GM. Results were however significantly different between the two known concentration phantoms (p = 0.001) for the short component only.

Table 2 shows the mean results from all volunteers grouped by WM and GM region. Fastest short and long T_2^* components are generally found in the periventricular WM (T_2^* = 2.5 ± 0.5 ms and 21.75 ± 7.45 ms) and for WM in the cerebellum (T_2^* = 2.5 ± 0.9 ms and 23.4 ± 3.7 ms). The slowest short and long T_2^* were found in the cerebral GM (T_2^*-short= 5.6 ± 0.9 ms and T_2^*-long=31 ± 3.7 ms). While no significant differences were found for the long components, the short T_2^* component for the frontal white matter differed significantly from all other regions of interest (p < 0.05). Periventricular white matter was also significantly different from deep grey matter (p < 0.05).

Continuous distribution fit

Figure 5 shows an exemplary signal decay plot and associated spectrum of relaxation times from a WM ROI. Figure 6 shows an exemplary decay and fit for a WM ROI exhibiting two closely spaced short components. The mean results over all WM and GM measures using the continuous distribution fit are shown in table 3. Where more than one distinct short T_2^* component was present (<5 ms), their amplitudes have been added up. WM, GM and phantoms had similar short (p>0.05) and long T_2^*'s (p>0.05).

Table 4 contains the results of the regularised inverse Laplace transform fit averaged for all volunteers and split into ROIs as in table 2 for the different WM and GM regions. The short

component result for frontal WM was significantly different from both cerebellar white and grey matter (p<0.005). No other statistically significant differences were found for the individual components and sub-classes of tissue types.

Discussion

While 23 Na-T_2^* investigations of the brain have been performed before, they either used insufficiently short echo times to accurately characterise the short T_2^* component or only published the short T_2^* component as the average for all tissue types within the human brain in a short conference submission. Bartha and Menon investigated the long ^{23}Na T_2^* component in the healthy human brain only, as they were using 10 echo times between 3.8 and 68.7 ms. Nevertheless they found the long component to vary significantly for different anatomical regions.[21] Fleysher et al. used a two-point protocol with echo times of 12 and 37 ms and found that the long T_2^* component in the healthy human brain tissue appears longer at 7T.[22] As part of a TQF study, Fleysher et al. reported a whole head triple quantum filtered short T_2^* relaxation rate of 2 ± 0.3 ms at 7T.[23] This compares well to our results given that T_2^* is expected to be slightly shorter at 7T. In a short conference submission, Lu et al. also found the long sodium T_2^* component to be different between healthy white and grey matter (WM and GM respectively), but only provided a range for the short component indiscriminate of the tissue type. The group also used a bi-exponential model with echo times in the range of 0.2 and 28.8 ms,[24] which do not cover all sodium T_2^* present in the brain, with cerebrospinal fluid T_2^* values previously found of around 60 ms.[11]

Both bi-exponential and continuous distribution fitting in the current study found mean T_2^*-estimates for the short component in WM and GM of around 3 ms. This shows the similarity in short T_2^* component for the mean values of the two tissue types. Similarly, the mean long T_2^* component for both tissue types was found to be of around 24 and 18 ms using the bi-exponential and continuous distribution fit respectively, with no statistically significant difference between the average time constants for both tissues. This is in disagreement with a previous study, which found the long component to be different between white and grey matter, despite the use of identical voxel size and similar echo times as in our study.[21] Average time constants for the long component do however differ between the two fitting methods, with it being of around 25 ms using the bi-exponential model, and around 18 ms using the continuous distribution model. Results for the long component using both methods fall into the ranges reported by previous studies.[21,22,24] While the bi-exponential fit results for the phantoms show a

minor (statistically significant) increase in short transverse relaxation time estimate for the higher concentration phantom, the results from the continuous distribution fit suggest the opposite, a reduction in short T_2^* component, albeit not statistically significant. Phantom results from both fits are within the reported ranges for this concentration of agar.[12]

Estimated T_2^* relaxation times were shorter for both short and long components using the regularised inverse Laplace transform fitting method, as compared to the bi-exponential NNLS fitting approach. Some trends such as a faster short component for periventricular WM and cerebellar tissue and a longer short component for frontal WM were observed for both fitting methods while parietal WM and deep GM were not comparable between the two fitting methods. At the resolution used, partial volume effects are to be expected, in particular for GM in the cerebral cortex, but should be minimal in the larger structures of the deep nuclei and WM in general.

Bi-exponential non-negative least squares fit

Short T_2^* component values from the two agar phantoms were significantly different, suggesting a link between T_2^* and sodium concentration, as they contained the same amount of agar and therefore should have similar environmental properties. However air bubbles could have had an effect on this measurement. A great variation of short and long T_2^* times is found between different areas of the brain, despite little sodium concentration differences associated with these tissue types.[1,25-27] In particular, both WM and GM short T_2^* are lower in the cerebellum, compared to other areas. The variation could be due to T_2^* being influenced by the different organisation of the tissue in these areas. Short T_2^* in periventricular WM, appears shorter than in other WM areas. This area has previously been shown to have a generally lower sodium concentration too, therefore suggesting a lower T_2^* due to the lower sodium concentration[1,25-27] or due to environmental properties of the highly ordered WM fibre tracts. Alternatively, looking at this as a "chicken and egg" problem, a short T_2^* can result in a low TSC value, as depending on the effective echo time used, some of the signal may have dephased before and during the readout, leading to underestimation of the true TSC. Larger standard deviations were found for the longer component for periventricular and cerebellar WM, which could be due to partial volume effects from CSF.

At 250Hz/pixel readout bandwidth, the corresponding readout length was 2 ms. This readout duration was chosen as it provided the best trade-off between echo spacing and SNR. Longer readouts would have provided better SNR at the expense of a weighting towards longer echo

times and longer ΔTE spacing. As the emphasis in this study was for characterisation of the short component, this decision was made during protocol set up. Larger measurement errors for the long component could stem from the readout duration being sub-optimal for long T_2 decay species and imperfections in the rephasing of the echo.

Continuous distribution fit

The SNR of the short and long component is also reflected in the continuous distribution fit by their respective peak widths, with the higher SNR short component displaying lower overall standard deviations with narrow distribution widths. The results confirm the findings of the bi-exponential fit. The large standard deviations on the amplitude ratio can be explained in part due to some ROIs where the amplitude-relationship between the long and short component (theoretically 60 and 40 %, respectively[11,12]) is reversed. While the amplitude reversal has been observed before in knee cartilage, it was in part attributed to B_0 inhomogeneities at 7T,[28] which would not entirely explain such a strong variation at 3T. Interactions with other macromolecules and ions, which are more present in some tissues rather than others, may also explain the deviation.[6]

Results for the long component of the agar phantoms are very similar to those reported by Madelin[28] while the short component results at 4 ms are longer than those reported by the same study, which however used 2-5 times higher sodium concentrations in the make-up of their phantom. Taken altogether, the results from both brain and phantoms show a relationship between sodium concentration and the short T_2^* component. Further investigation is needed to assess whether the short component could show sensitivity to concentration, and the long component to organisation and sodium environment. Schepkin et al. also report a correlation between sodium concentration and T_2^* due to competitive binding effects of potassium and other ions.[6]

Around 50 % of the samples exhibit two closely spaced or overlapping short distributions, with values between 0.3-1.5 ms centred on one side, and slightly longer values of 2-5 ms on the other side. While this explains slightly lower short T_2^* estimates from the continuous distribution fit as compared to the bi-exponential fit, it has to be carefully investigated whether this observance displays a true additional component or is a fitting or data related issue. Values as short as 0.3 ms have previously only been found in the cartilage of the knee joint, an arguably denser, more restrictive tissue environment, than most that can be found in the brain. The extra component is likely to arise from partial volume of an additional tissue species with a much faster short T_2^* component and indistinguishable long component, due to the decreased SNR at

longer echo times. Further investigation is needed to ascertain whether [23]Na-MRI T_2^* estimation could be sensitive enough to distinguish several T_2^* related tissue types within a voxel. However, at the SNR experienced in [23]Na-MRI, continuous distribution function modelling such as through the regularised inverse Laplace transform as performed here, becomes increasingly unstable and could produce non-physical results from residuals and noise. The additional short component was also present in the phantoms, which provides a more reproducible measure, however an investigation with higher SNR phantoms such as those using higher NaCl concentrations is warranted, and results should be compared to those from multiple quantum filtered experiments. While due experimental care was taken in protocol design and data post-processing, the fact that the data-sets were obtained using 4 separate (but subsequent, same-session) scans and subsequent realignment of the images could have also be a factor in the observance of two short T_2^* components, and further verification could be performed using an improved protocol design and higher field strength. Continuous distribution fitting has the potential to disentangle different intracellular compartments such as the cell nucleus versus the cytoplasm. However, due care needs to be taken, as the underlying mathematical problem is an ill-posed one.[14,15,18]

No additional long components, such as the ones potentially coming from cerebrospinal-fluid contamination within an ROI were found. Care was taken to particularly minimise partial volume within an ROI, however due to lower SNR at longer echo times, long T_2^* CSF contamination may have not been picked up by the fit.

Conclusion

We present for the first time [23]Na T_2^* values of the brain for the short and long component for various anatomical locations using ultra-short echo times. To my knowledge, this is also the first time that [23]Na T_2^* estimates have been obtained using a continuous distribution model. Both fitting techniques used in this study were found to yield similar results. The short [23]Na T_2^* appears shorter for regions of low estimated tissue sodium concentration such as in the periventricular white matter, and longer in grey matter, which has previously been found to contain more apparent tissue sodium.[1,25-27] While some of the results suggest a relationship between [23]Na concentration, others could not be explained by previously found concentration differences, and may suggest an additional environmental effect on the [23]Na T_2^* such as interactions with potassium or chloride ions.[6] The small standard deviations found for the short

component offer the prospect for comparison between healthy and diseased tissue, warranting possible new insight in brain diseases such as Multiple Sclerosis.

Acknowledgments

References

1. Inglese M, Madelin G, Oesingmann N., Babb JS, Wu W, Stoeckel B, Herbert J, Johnson G. Brain tissue sodium concentration in Multiple Sclerosis: a sodium imaging study at 3 Tesla. BRAIN 2010;133:847-857.

2. Mellon EA, Pilkinton D, Clark CM, Elliott MA, Witschey WR 2nd, Borthakur A, Reddy R. MR imaging detection of mild Alzheimer disease: Preliminary Study. Am J Neuroradiol. 2009;30:978–984.

3. Reetz K, Romanzetti S, Dogan I, Sass C, Werner CJ, Schiefer J, Schulz JB, Shah NJ. Increased brain tissue sodium concentration in Huntington's Disease—a sodium imaging study at 4T. Neuroimage. 2012;63(1):517–524.

4. Benkhedah N, Bachert P, Nagel AM. Two-pulse biexponential-weighted 23Na imaging. J Magn Reson 2014;240:67–76.
5. Madelin G, Kline R, Walvick R, Regatte RR. A method for estimating intracellular sodium concentration and extracellular volume fraction in brain in vivo using sodium magnetic resonance imaging. Sci Rep 2014;4:4763.

6. Schepkin VD, Neubauer A, Nagel AM, Budinger TF. Comparison of potassium and sodium binding in vivo and in agarose samples using TQTPPI pulse sequence. J Magn Reson 2017;277:162-168.

7. Fleysher L, Oesingmann N, Brown R, Jaggi H, Wiggins GC, Sodickson D, Inglese M. Intra-cellular sodium concentration and intra-cellular volume fraction quantification in the human brain using 7T MRI in-vivo. In Proceedings of the 19th Annual Meeting of ISMRM, Montreal, Quebec, Canada, 2011. p. 1709.

8. Fleysher L, Oesingmann N, Brown R, Jaggi H, Wiggins GC, Sodickson D, Herbert J, Inglese M. Multiple Sclerosis alters intra-cellular sodium concentration and intra-cellular volume fraction: an in-vivo 7T MRI study. In Proceedings of the 19th Annual Meeting of ISMRM, Montreal, Quebec, Canada, 2011. p. 604.

9. Madelin G, Oesingmann N, Johnson G, Jerschow A, Inglese M. Sodium MRI with triple quantum filter and inversion recovery at 7T. In Proceedings of the 16th Annual Meeting of ISMRM, Toronto, Ontario, Canada, 2008. p. 3251.

10. MacKay A, Whittall K, Adler J, Li D, Paty G, Graeb D. In vivo visualization of myelin water in brain by magnetic resonance. Magn Reson Med 1994;31:673-677.

11. Madelin G, Regatte RR. Biomedical applications of sodium MRI in vivo. J Magn Reson Imaging 2013;38:511-529.

12. Woessner DE. NMR relaxation of spin-3/2 nuclei: effects of structure, order, and dynamics in aqueous heterogeneous systems. Concepts Magn Reson 2001;13(5):294–325.

13. Rahmer J, Börnert P, Groen J, Bos C. Three-dimensional radial ultrashort echo-time imaging with T2 adapted sampling. Magn Reson Med 2006;55:1075–1082.

14. Provencher SW. A constrained regularization method for inverting data rep- resented by linear algebraic or integral equations. Comput Phys Commun 1982;27:213–227

15. Provencher SW. A general purpose constrained regularization program for inverting noisy linear algebraic and integral equations. Comput Phys Commun 1982;27:229–242.

16. Woessner DE. NMR relaxation of spin-3/2 nuclei: effects of structure, order, and dynamics in aqueous heterogeneous systems. Concepts Magn Reson 2001;13(5):294–325.

17. Miller AJ, Joseph PM. The use of power images to perform quantitative analysis on low SNR MR images. Magn Reson Imaging 1993;11:1051–1056.

18. Marino IG. MathWorks MATLAB Central File Exchange: rilt - Regularized Inverse Laplace Transform Web site. http://www.mathworks.com/matlabcentral/fileexchange/6523-rilt. Published December 10, 2004. Updated May 10, 2007. Accessed April 22, 2015.

19. Menon RS, Allen PS. Application of continuous relaxation time distributions to the fitting of data from model systems and excised tissue. Magn Reson Med 1991;20:214-227.

20. Kroeker RM, Henkelman RM. Analysis of Biological NMR Relaxation Data with Continuous Distributions of Relaxation Times. J Magn Reson 1986;69:218-235.

21. Bartha R, Menon RS. Long component time constant of 23Na T2* image relaxation in healthy human brain. Magn Reson Med 2004;52:407–410.

22. Fleysher L, Oesingmann N, Stoeckel B, Grossman RI, Inglese M. Sodium long-component T2* mapping in human brain at 7 Tesla. Magn Reson Med 2009;62:1338–1341.

23. Fleysher L, Oesingmann N, Brown R, Sodickson DK, Wiggins GC, Inglese M. Noninvasive quantification of intracellular sodium in human brain using ultrahigh-field MRI. NMR Biomed 2013;26:9–19.

24. Lu A, Atkinson IC, Thulborn KR. In vivo sodium T2* mapping with a multiple-echo flexible TPI sequence. In Proceedings of the 19th Annual Meeting of ISMRM, Montreal, Quebec, Canada, 2011. p. 3504.

25. Zaaraoui W, Konstandin S, Audoin B, Nagel AM, Rico A, Malikova I, Soulier E, Viout P, Confort-Gouny S, Cozzone PJ, Pelletier J, Schad LR, Ranjeva JP. Distribution of brain sodium accumulation correlates with disability in multiple sclerosis: a cross-sectional 23Na MR imaging study. Radiology 2012;264:859–867.

26. Maarouf A, Audoin B, Konstandin S, Rico A, Soulier E, Reuter F, Le Troter A, Confort-Gouny S, Cozzone PJ, Guye M, Schad LR, Pelletier J, Ranjeva JP, Zaaraoui, W. Topography of brain sodium accumulation in progressive multiple sclerosis. Magn Reson Mater Phys 2014;27:53-62.

27. Paling D, Solanky BS, Riemer F, Tozer DJ, Wheeler-Kingshott CA, Kapoor R, Golay X, Miller DH. Sodium accumulation is associated with disability and a progressive course in Multiple Sclerosis. BRAIN 2013;136:2305-2317.

28. Madelin G, Jerschow A, Regatte RR. Sodium relaxation times in the knee joint in vivo at 7T. NMR Biomed 2012;25:530-537.

Tables

Table 1

Average WM, GM and phantom T_2^* estimates from all volunteers using the bi-exponential fixed fraction NNLS fit

Region (average)	Short T_2^* component (ms)	Long T_2^* component (ms)
White Matter (WM)	3.4 ± 0.2	23.5 ± 1.8
Grey Matter (WM)	3.9 ± 0.5	26.3 ± 2.6
33 mM/l NaCl in 4% agar	5.2 ± 0.5	23.2 ± 1.7
66 mM/l NaCl in 4% agar	6.4 ± 0.3	21.9 ± 1.6

Table 2

Average WM and GM T_2^* from all volunteers, divided into ROIs for the main lobes, cerebellar cortex (GM only) and cerebellum using the bi-exponential fixed fraction NNLS fit

Region of Interest	Short T_2^* component (ms)	Long T_2^* component (ms)
Frontal WM	3.5 ± 0.25	23.6 ± 1.8
Periventricular WM	2.5 ± 0.45	21.75 ± 7.45
Parietal WM	3.5 ± 0.3	23.2 ± 1.4
Occipital WM	3.6 ± 0.4	24.7 ± 2.2
Cerebellar WM	2.5 ± 0.9	23.4 ± 3.7
Deep GM	3.6 ± 0.4	24.8 ± 2.3
Cerebral GM	5.6 ± 0.9	31 ± 3.7
Cerebellar GM	3.3 ± 0.5	25.5 ± 5.75

Table 3

Mean WM and GM short and long T_2^* components and their respective amplitudes with associated standard deviations[a]

Region (average)	Short T_2^* component (ms)	Short T_2^* component amplitude (1...100)	Long T_2^* component (ms)	Long T_2^* component amplitude (1...100)
White Matter (WM)	3.1 ± 0.3	61.1 ± 18.2	18.8 ± 3.2	38.9 ± 13.7
Grey Matter (GM)	2.9 ± 0.4	49.4 ± 13.1	17.2 ± 2.0	50.6 ± 16.0
33 mM/l NaCl in 4% agar	4.0 ± 1.1	55.0 ± 17.2	15.0 ± 1.2	45.0 ± 12.1
66 mM/l NaCl in 4% agar	3.6 ± 0.5	57.1 ± 13.3	12.1 ± 3.4	42.9 ± 18.5

[a]Peak decay times were used only and the amplitudes are given as the sum of all components within a distribution. Amplitudes may not add to a hundred percent due to rounding.

Table 4

Average WM and GM T_2^* from all volunteers, divided into ROIs for the main lobes, cerebellar cortex (GM only) and cerebellum using the regularised inverse Laplace transform fit

Region of Interest	Short T_2^* Component (ms)	Short T_2^* Component Amplitude (1...100)	Long T_2^* Component (ms)	Long T_2^* Component Amplitude (1...100)
Frontal WM	3.7 ± 1.1	70.2 ± 29	18.5 ± 4.8	29.8 ± 11.6
Periventricular WM	2.5 ± 0.5	90.3 ± 4.0	22.2 ± 9.0	9.7 ± 4.0
Parietal WM	2.7 ± 0.6	78.0 ± 21.0	17.8 ± 6.0	22.0 ± 7.6
Occipital WM	3.1 ± 0.4	61.5 ± 28.5	18.2 ± 4.0	39.5 ± 3.6
Cerebellar WM	2.4 ± 0.6	66.8 ± 32.5	15.5 ± 5.2	33.2 ± 23.4
Deep GM	2.6 ± 0.6	47.7 ± 21.7	17.7 ± 3.2	52.3 ± 16.5
Cerebral GM	3.3 ± 1.2	42.4 ± 19.2	16.7 ± 3.1	57.6 ± 15.2
Cerebellar GM	2.3 ± 1.1	66.3 ± 20.1	16.5 ± 5.3	33.7 ± 8.7

Figures
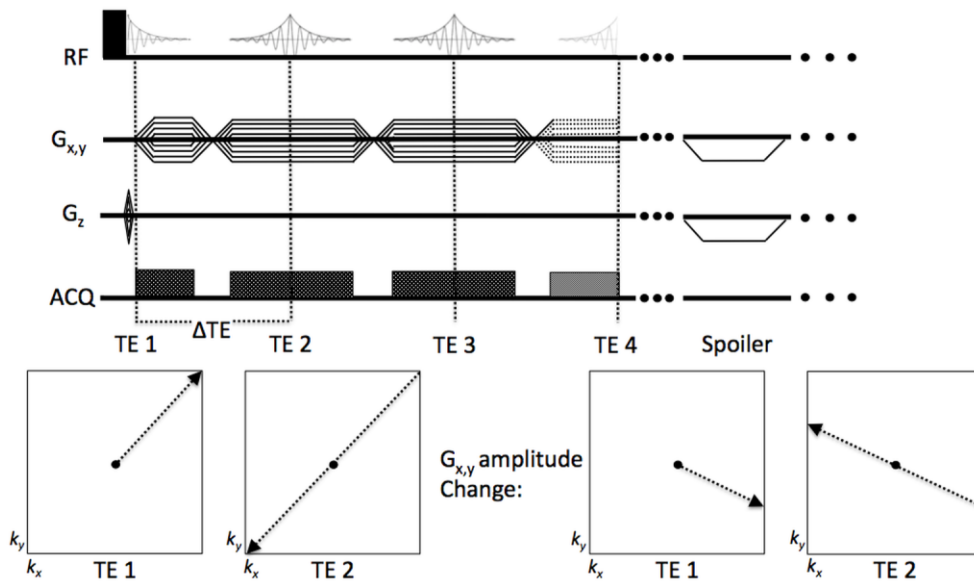
FIG. 1. Illustration of the pulse sequence used for acquisition of the radial multi-echo scan. After the FID with minimal delay (TE = 0.17 ms) has been sampled, 15 echoes (ΔTE = 4.7 ms) are acquired and G_X and G_Y are incremented in subsequent readouts (top). While for the FID only half a line in k-space is acquired, each echo samples a full line in k-space (bottom). Short echo times of 0.3, 0.5 and 1 ms were acquired using additional scans with FID-only readouts.
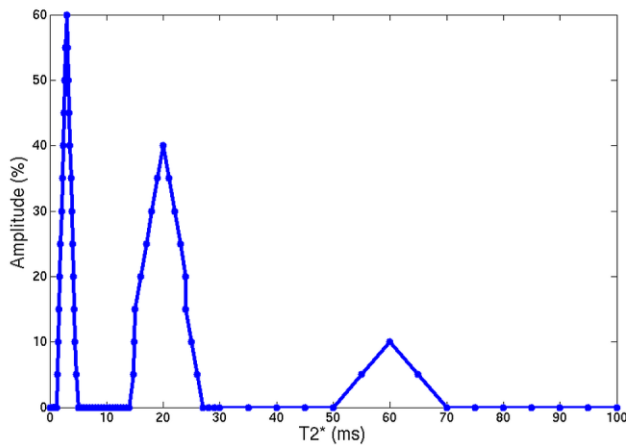

FIG. 2. Initial guess distribution supplied to the fitting algorithm. Initial T_2^* times and amplitudes were supplied according to (11).
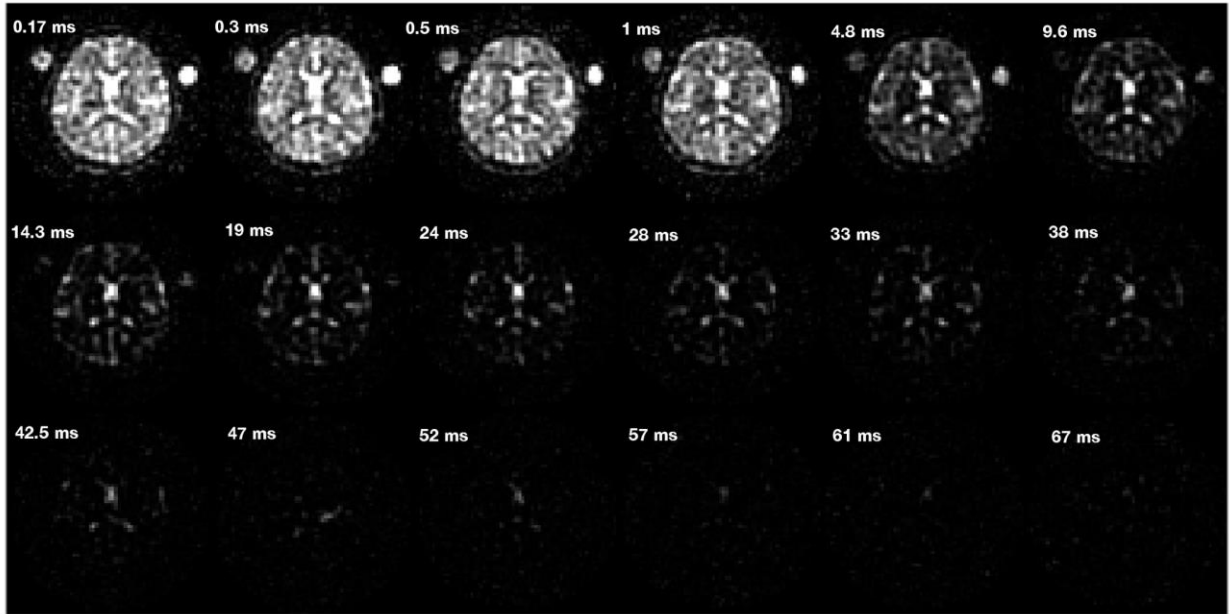
FIG. 3. Transverse section of the brain at the height of the lateral ventricles from one volunteer, shown for the different echo times used in the study. Shortest echo time (0.17 ms) is shown in the top left, increasing row-wise to the longest echo time shown in the bottom right (70.7 ms). Signal from the phantoms and white and grey matter is becoming completely absent after the 7th echo time (14.3 ms), whereas signal from the central ventricular space is still discernible at the 16th echo time (56.7 ms).
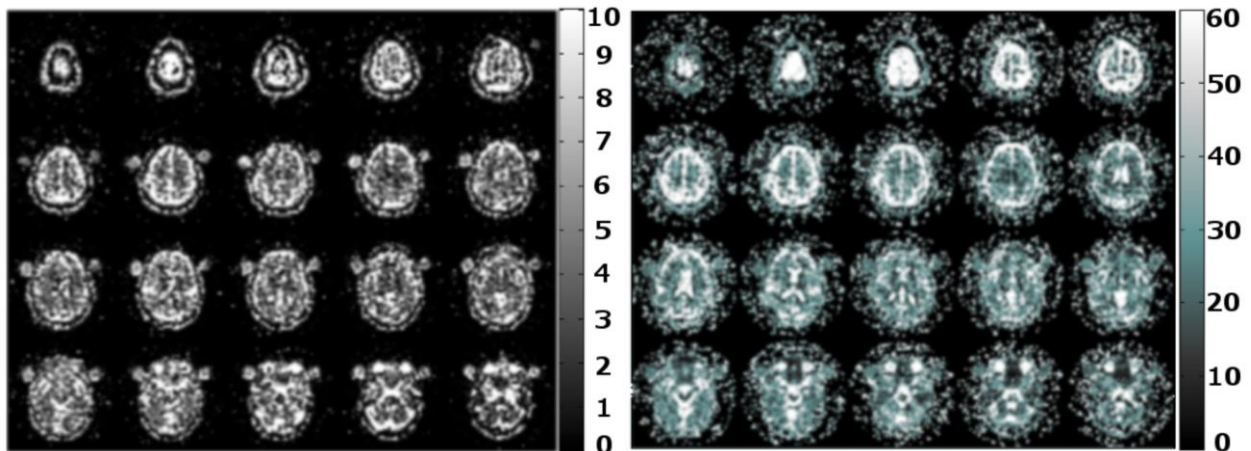

FIG. 4. Whole brain T_2^* component maps (scale ms). The left-hand side shows the high amplitude, short T_2^* component. On the right-hand side the smaller amplitude long T_2^* component is shown. Colour bar and scale representative of range of T_2^* estimates found for
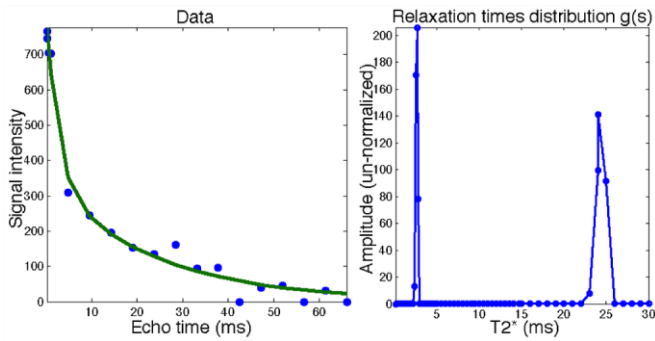
each component.

FIG. 5. Plot of decay signal from a WM region of interest (left) and resultant relaxation time spectrum (right), showing a high amplitude short component of small linewidth and a long component of smaller amplitude and broader linewidth.
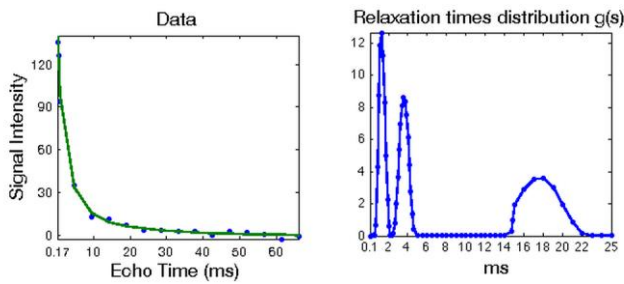

FIG. 6. Plot of decay signal from a WM region of interest (left) and resultant relaxation time spectrum (right) with two closely spaced short T_2^* component peaks. About 50 % of the analysed regions of interest exhibited two overlapping or closely space short T_2^* component peaks.